18

Applications of the Planar Fiber Optic Chip

Brooke M. Beam[1], Jennifer L. Burnett[2],
Nathan A. Webster[2] and Sergio B. Mendes[2]
[1]*University of Arizona*
[2]*University of Louisville*
USA

1. Introduction

The planar fiber-optic chip (FOC) technology combines the sensitivity of an attenuated total reflection (ATR) element with the ease of use of fiber-optic based spectrometers and light sources to create an improved platform for spectroscopic analysis of molecular adsorbates. A multi-mode optical fiber mounted in a V-groove block was side-polished to create a planar platform that allows access to the evanescent field escaping from the fiber core and has been previously applied to absorbance and spectroelectrochemical measurements of molecular thin-films. Light generated in a surface-confined thin molecular film can be back-coupled into the FOC platform when the conditions for light propagation within the waveguide are met. In this chapter the current applications of the FOC platform will be presented including spectroelectrochemical measurements, fluorescence detection of a bioassay, a broadband fiber optic light source, and Raman interrogation of molecular adsorbates.

In recent years, both planar waveguide-based and fiber-optic-based chemical sensors and biosensors have been developed in an attempt to meet the need for miniature, multifunctional, and sensitive sensor platforms. (Bradshaw *et al.*, 2005; Kuswandi *et al.*, 2001; Monk & Walt, 2004; Plowman *et al.*, 1998; Potyrailo *et al.*, 1998; Reichert, 1989; Tien, 1971; Wolfbeis, 2006) The benefits of fiber optic platforms have led several manufactures of analytical instrumentation to develop inexpensive fiber compatible equipment such as readily available fiber-coupled light sources and spectrometers with standard distal end fiber coupling schemes. Fiber coupled sensing architectures, utilizing the fiber as the optical signal transduction platform, have been developed for various geometries including distal end, tapered, de-clad cylindrical core, U-shape de-clad cylindrical core, and biconical tapered optical fibers. (Leung *et al.*, 2007; McDonagh *et al.*, 2008) Simple distal end fiber optic sensors are commercially available where the exposed core on a cleaved and polished end of a fiber is used as the sensing platform. However, the distal end geometry is limited by low sensitivity due to the small interaction area, analogous to the single-pass transmission absorbance measurement. A second more fragile distal end sensor geometry uses a tapered fiber where the fiber core is etched with HF into a point. The tapered fiber increases the evanescent field amplitude and penetration depth, thus increasing the sensitivity of the platform. Tapered fiber optic sensors are primarily used as fluorescence detection platforms in biochemical and clinical applications. (Anderson *et al.*, 1993; Anderson *et al.*, 1994; Anderson *et al.*, 1994; Golden *et al.*, 1992; Grant & Glass, 1997; Maragos & Thompson, 1999; Thompson & Maragos, 1996; Wiejata *et al.*, 2003; Zhou *et al.*, 1997)

Previous studies, which have taken advantage of the convenience of fiber coupled instrumentation and the increased sensitivity of the total internal reflection geometry, have used a fiber optic with the cladding removed to create a sensing element around the cylindrical fiber core. The exposed core region serves as an ATR element that can be used for absorbance measurements to detect volatile organic compounds (Blair *et al.*, 1997), probe dye solutions (Ruddy *et al.*, 1990), monitor methane gas (Tai *et al.*, 1987) and ammonium ion (Malins *et al.*, 1998) concentrations, and determine solution pH using indicator doped sol-gel coatings (Gupta & Sharma, 1997; MacCraith, 1993), or an indicator doped polymer film. (Egami *et al.*, 1996) Several investigators have worked to further increase the sensitivity of the de-clad cylindrical core fiber optic sensors by tapering the fiber optic (Guo & Albin, 2003; Gupta *et al.*, 1994; Mackenzie & Payne, 1990; Mignani *et al.*, 1998) or bending the sensing region (i.e. into a U-shape). (Khijwania & Gupta, 1998; Khijwania & Gupta, 2000) Fiber optic sensors using the tapered fiber geometry include a humidity (Bariain *et al.*, 2000), temperature (Diaz-Herrera *et al.*, 2004), hydrogen gas (Villatoro *et al.*, 2005), and bovine serum albumin sensors. (Leung *et al.*, 2007; Preejith *et al.*, 2003) U-shaped fiber optic sensors have been used to detect humidity (Gupta & Ratnanjali, 2001), pH (Gupta & Sharma, 2002), and ammonium ion concentrations. (Potyrailo & Hieftje, 1998) Such fiber optic sensor architectures employ signal transduction through a fragile cylindrical probing interface, which can be problematic for several applications where a robust platform or planar deposition technologies are required. Clearly, a supported planar interface would be advantageous for using standard planar deposition technologies such as Langmuir-Blodgett (LB)-deposited thin-films (Doherty *et al.*, 2005; Flora *et al.*, 2005) and planar supported lipid bilayers. (McBee *et al.*, 2006) In addition, due to its more robust supported platform, a planar design would be amenable for integration into microfluidic systems and sensor arrays. The FOC platform is schematically shown in Figure 1.

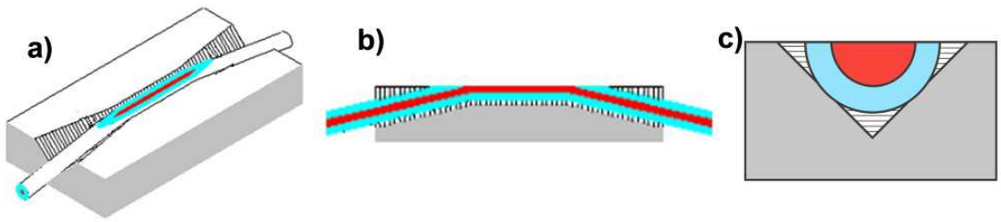

Fig. 1. Fiber Optic Chip (FOC) schematic of a side polished fiber mounted in a V-groove where red represents the exposed fiber core sensing platform. a) Top down view; b) Side view; c) Cross section. Figure modified from Beam *et al.*, 2007 and Beam *et al.*, 2009.

1.1 FOC manufacture

The FOC is a D-shaped, side polished fiber optic platform with access to the evanescent field escaping from the fiber core. Fabrication of the FOC begins with stripping the jacket off of a small central section, 2 to 4 cm, of an optical fiber to expose the cladding. The optical fibers used for this work are a 50 μm core/125 μm cladding multimode, step-index optical fiber (Thorlabs AFS50/125Y), with 0.22 numerical aperture (NA). The stripped section of the optical fiber is then mounted in a V-groove substrate using a two-part epoxy; the V-groove acts as a platform for spectroscopic investigation as well as supports the fragile fiber during the polishing proceedure. Prior to mounting the fiber, the edges of the V-groove block must be polished to a 2° taper. Using a custom built assembly jig to keep tension on the fiber

during hotplate curing, the fiber is laid into the V-groove and optical grade epoxy (Epotek 301) is applied liberally to ensure permanent immobilization of the fiber. The first generation FOC platforms were produced by side-polishing an optical fiber in a glass V-groove mount, but subsequent improvements on the FOC manufacturing process include replacing the glass V-groove with a customized etched silicon wafer support, improved polishing processing, and finally generating arrays of side polished fibers (Figure 2).

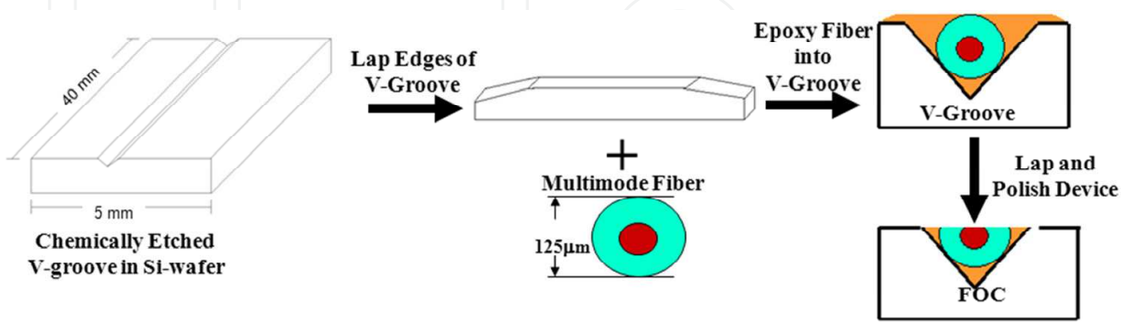

Fig. 2. Schematic for construction of FOC devices.

Initially glass V-groove mounts were purchased from Mindrum with dimensions of 40 mm long, 2 mm wide, and 1.33 mm tall; however, there was a limited supply and the glass V-grooves were not uniform requiring careful charaterization of each piece prior to use. Later V-groove mounts were produced using a chemical etching process (Kendall, 1979) to create a channel in a Si-wafer. Due to the crystalline structure of silicon, the resultant channel has two sloping walls forming a V shape. Creating the V-groove begins with a 500 µm thick Si-wafer with a minimum of a 1 µm oxidized layer. A layer of hexamethyldisilazane (HMDS) primer followed by a layer of photo-resist (Shipley 1813) is spin-coated on the wafer and cured on a hot plate. A slotted mask is placed on top of the wafer using a mask aligner (Süss MicroTec). The slots are of the desired width for the eventual V-groove. The masked wafer is then exposed to UV light for 7 seconds. The wafer is then placed in developer (Microdeposit MF-319) leaving photo-resist in the areas that the mask covered and exposing the wafer surface in the slot formation. The wafer is covered in buffered oxide etchant (BOE) to erode the oxide layer of the exposed wafer, etching the masked pattern into the oxide layer. The BOE will remove 100nm/min of the oxidized layer, so at minimum the wafer should remain in the BOE for a period of 10 minutes. The remaining photo-resist is then removed using a solvent rinse. Finally, the V-grooves are formed through chemical etch in 45% KOH, which is set on a magnetic stirrer and heated to 55° C. It should be noted that the etching rate of the KOH increases with temperature. The KOH etches the silicon at a much faster rate than the SiO_2 creating grooves only in the areas without an oxidized layer. The angle between the sloping walls and the face of the substrate, 54.74°, is set by the silicon crystalline structure. Etching will terminate once the (1,1,1) plane is reached; therefore, the depth of the V-groove is pre-determined by the width of the lines in the mask. The resultant V-groove is approximately 240 µm wide and 170 µm deep. Once the chemical etching of the V-grooves is complete, the Si-wafer is diced into approximately 40 mm by 5 mm long strips with a V-groove running longwise through the center of each or the wafer can remain intact to create a FOC array base structure.

Side polishing the fiber to create the D-shaped geometrey of the FOC is achieved using a two part lapping process, where the cladding is slowly polished away exposing the core of

the multimode fiber. All lapping and polishing steps are performed on a Lapmaseter model 12 with a cast iron lapping plate covered with a polyurethane pad. The FOC device is mounted onto a custom machined spindle carrier with brass sleeve bearings to hinder parallax motion. If this wobble is not corrected for, the FOC will not be polished evenly leading to the outer edges eroding at a faster rate. First, a coarse grit slurry composed of 1% 1-μm alumina powder (MetMaster SF-RF-1P) is used to lap the device at a rate of about 20 rpm. When the measured width of the exposed cladding is approximately 115 μm, the slurry is changed to a fine grit polishing solution composed of 1% 0.5-μm cerium oxide (Logitech OCON 260). Polishing continues until the center of the fiber is reached, measuring approximately 125 μm across the width of the exposed cladding. Once lapping is complete, FC-PC connectors are attached to the optical fiber ends on both sides of the device.

The sensitivity of an FOC device is intrinsically dependent upon the specific geometry of the side-polished fiber. The fundamental limit of the elliptical flattened area is determined by the structure of the V-groove mount, evenly mounting the fiber in epoxy, and the efficiency of exposure of the fiber core through the polishing process. The depth to which the fiber has been polished is determined by measuring the width of exposed fiber. The width of the fiber is monitored using a standard optical microscope (VWR Vista Vision) and periodically measuring from the boundary of the cladding and epoxy on either side of the fiber. Measurements are taken periodically throughout the lapping process to ensure the fiber is polishing evenly.

1.2 Broadband absorbance measurements on the FOC platform

The initial application of the FOC platform was to examine the broadband absorbance characteristics of molecular thin-films. A schematic of the experimental set-up for general absorbance measurements on the FOC is shown in Figure 3a. The thin-film absorbance sensitivity enhancement of the FOC device was evaluated and compared to previously existing technologies. The sensitivity factor (S) of a device, defined in Equation 1, is a scaling factor of the device absorbance (A_{FOC}) with respect to the conventional absorbance measured ($A_{transmission}$) in direct transmission and used to quantify the sensitivity enhancement of the FOC and ATR platforms.

$$S \equiv \frac{A_{FOC,film}}{A_{transmission}} = \frac{A_{FOC,film}}{\varepsilon_{film}\,\Gamma_{film}} \tag{1}$$

Where ε is the molar absorptivity and Γ is the molecular surface coverage of the film under test. Absorbance of a polyion self-assembled film of poly (diallyldimethylammonium chloride) (P+) and Nickel (II) phthalocyaninetetrasulfonic acid (Ni (TSPc)) on both the FOC and ATR (Doherty *et al.*, 2002) platforms were used to compare the sensitivity perfomance of the two techniques. Figure 3b shows a comparison of the P+/Ni (TSPc) absorbance spectra on the ATR and FOC normalized by interaction length. Currently, the FOC yields thin-film absorbance values comparable with ATR instrumentation; however, the FOC eliminates the complex coupling optics and alignment procedures required to make such measurements using ATR instrumentation. (Beam *et al.*, 2007)

Further refinements in the FOC platform promise to substantially increase its sensitivity. The lower order modes of a fiber (those with optical rays propagating at a small angle from the fiber axis and described by a greater effective refractive index, N) do not provide a

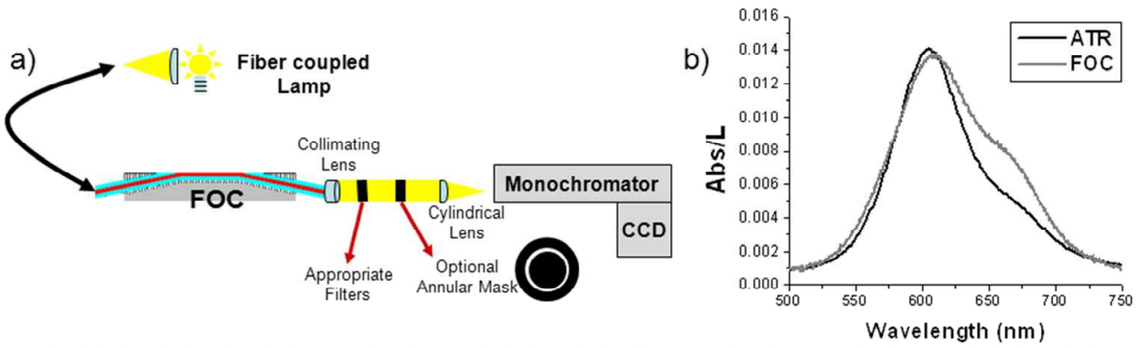

Fig. 3. a) Instrument schematic for FOC absorbance measurements. b) Spectra are of a self-assembled polyion film of P+ and Ni (TSPc), and the spectra are normalized by their interaction length (*L*) of 44 mm (for the ATR spectra) and 17.2 mm (for the FOC spectra). Modified from Beam *et al.*, 2007.

strong interaction with the molecules adsorbed on the active surface of the FOC. Removing these lower order modes from the optical beam prevents collecting average absorbance measurements which are unduly weighted toward the less sensitive traveling waves inside the fiber. (Gloge, 1971; Ruddy *et al.*, 1990) To select the modes allowed to propagate in the FOC an annular mask that only transmits a ring of light of a defined angle has been used. A mask delivering light with a low effective index, therefore working only with the highest order modes that the fiber can support, was shown to double the measured thin-film absorbance on the FOC compared to that measured for the same film without a mask. (Beam *et al.*, 2007)

1.3 The electroactive-fiber optic chip (EA-FOC)

Spectroelectrochemical measurements provide complimentary spectroscopic and electrochemical analytical data which have found applications using fiber coupled techniques. UV-Vis (VanDyke & Cheng, 1988), FTIR (Shaw & Geiger, 1996), and Raman (Hartnagel *et al.*, 1995) fiber coupled spectroelectrochemical measurements have been obtained using the distal end of a fiber optic probe as the working electrode. These fiber optic probes, however, suffer from the limited optical pathlength of transmission absorbance spectroelectrochemical measurements. Over the last decade the sensitivity of spectroelectrochemical measurements has been significantly enhanced by using monochromatic and broadband ATR platforms, (Doherty *et al.*, 2002; Winograd & Kuwana, 1969) multi-mode waveguides, and single-mode waveguides. (Bradshaw *et al.*, 2003; Dunphy *et al.*, 1997; Dunphy *et al.*, 1999; Itoh & Fujishima, 1988) A significant hindrance for these ATR and waveguide based spectroelectrochemical technologies has been interfacing the sensor platform with standard, commercially available spectroscopic instrumentation; thus, only one field portable instrument has been developed by Heinemann and coworkers to spectroelectrochemically detect ferrocyanide. (Monk *et al.*, 2002; Stegemiller *et al.*, 2003)

The first application of the FOC as a fully integrated fiber coupled spectroelctrochemical platform, was termed the electroactive-fiber optic chip (EA-FOC). To create the EA-FOC we coat the FOC with a thin-film of indium-tin oxide (ITO) as the working electrode (Figure 4a) and probe electrochemically driven changes in absorbance for surface confined redox species.

(Beam *et al.*, 2009) The sensitivity enhancement of the EA-FOC platform is calculated using the methylene blue (MB) redox couple. Additionally, the properties of the EA-FOC are demonstrated by probing the redox spectroelectrochemistry of an electrodeposited film of the conducting polymer poly (3,4-ethylenedioxythiophene) (PEDOT).

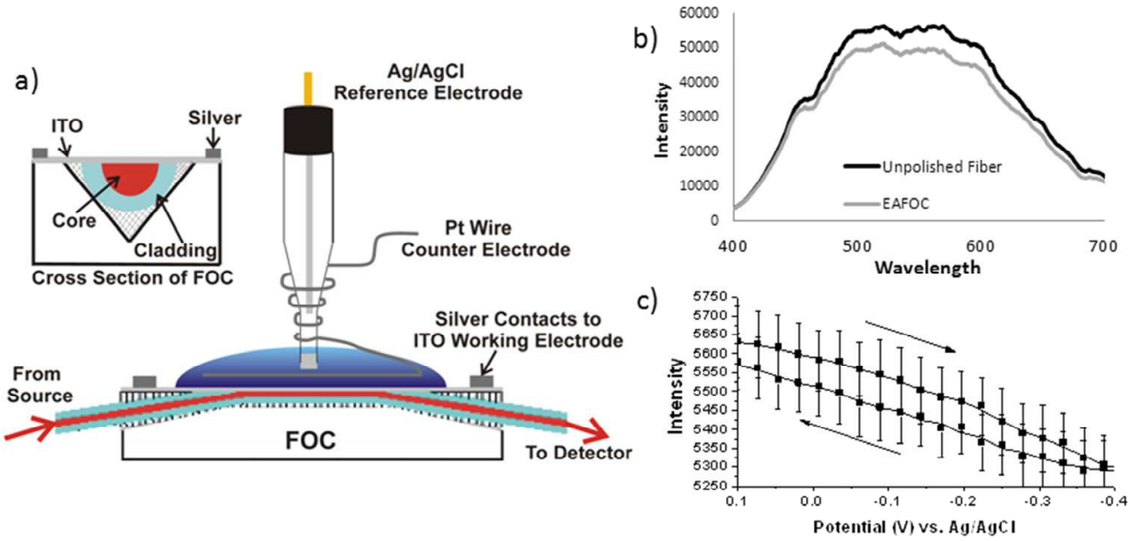

Fig. 4. The EA-FOC a) Schematic of the EA-FOC with labeled electrical contacts and a cross section (inset) b) comparison of the transmission spectra of an unpolished fiber with that of the EA-FOC and c) the EA-FOC out-coupled intensity as a function of potential at 665 nm in a 0.1M KNO_3 aqueous solution. Modified from Beam *et al.*, 2009.

1.3.1 Optical effects of ITO on the FOC

The optical properties of ITO are dependent on the electrochemical properties of the material. ITO is generally transparent in the visible region where the short wavelength cut off is determined by absorption due to the band gap of the material. The long wavelength cut off is due to scattering of free electrons and is determined by the plasma resonance frequency. As the free carriers within the material increases the plasma resonance wavelength decreases. Therefore, there is a trade off between increasing the free carrier concentration of ITO to improve the electrical properties and decreasing the transmission wavelength window. (Hartnagel *et al.*, 1995) For the ITO sputtered onto the FOC device, the minimum absorptivity coefficient was estimated to be 5×10^{-3} at 500 nm (or a propagation loss of ~ 0.5 dB/cm). The transmission of the ITO film on the FOC will affect the optical properties of the device platform, and the broadband transmission of the EAFOC device is slightly decreased by the addition of ITO (Figure 4b).

Before discussing spectroelectrochemical measurements made on the EA-FOC, it is important to evaluate the optical background of the device. Figure 4c plots the out-coupled intensity from the EA-FOC versus potential in an electrolyte solution without electrochemically active analytes. The linear decrease of intensity with potential is attributed to a change in the ITO absorptivity, which is due to the increase in free carrier concentration within the film as the applied potential decreases. To account for the affect of applied potential on the background signal of the EA-FOC, absorbance measurements at each

potential were calculated from solvent blanks recorded at a corresponding potential. Additionally, there is a slight hysteresis between the forward and backward potential sweeps due to ion diffusion. Equilibration of the ITO electrode in the electrolyte solution after 10 potential scans stabilized the magnitude of the hysteresis allowing analytical measurements to be collected.

1.3.2 Spectroelectrochemical measurements

The spectroelectrochemistry of adsorbed monolayers of methylene blue (MB) has been previously evaluated on both the ATR (Itoh & Fujishima, 1988) and waveguide-based (Dunphy *et al.*, 1997) platforms; therefore, the MB redox couple is used to compare the EA-FOC measurements with these well-known techniques. MB electrostatically adsorbs to the ITO surface in its native oxidized form. The surface adsorbed MB undergoes a chemically reversible 2-electron reduction to the transparent leuco form of the dye at ~ - 0.27 V versus a Ag/AgCl reference electrode. For the micromolar solution concentrations used in this study, the bulk MB absorbance does not contribute appreciably to the EA-FOC spectroelectrochemical response. Potential dependent spectra of MB on the EA-FOC (Figure 5a) shows absorbance maxima for both the monomer (665 nm) and aggregate forms of this dye (605 nm). (Bergmann & O'Konski, 1963) Simultaneous optical and electrochemical detection of the MB redox couple allow for the calculation of the sensitivity of the EA-FOC using the the electrochemically determined surface coverage and the experimentally measured absorbance, using the Beer's Law relationship in equation 1. The sensitivity of the EA-FOC was calculated to be 40 ± 2 or 20.6/cm, which is comparable to sensitivities calculated for the FOC devices. (Beam *et al.*, 2009; Beam *et al.*, 2007).

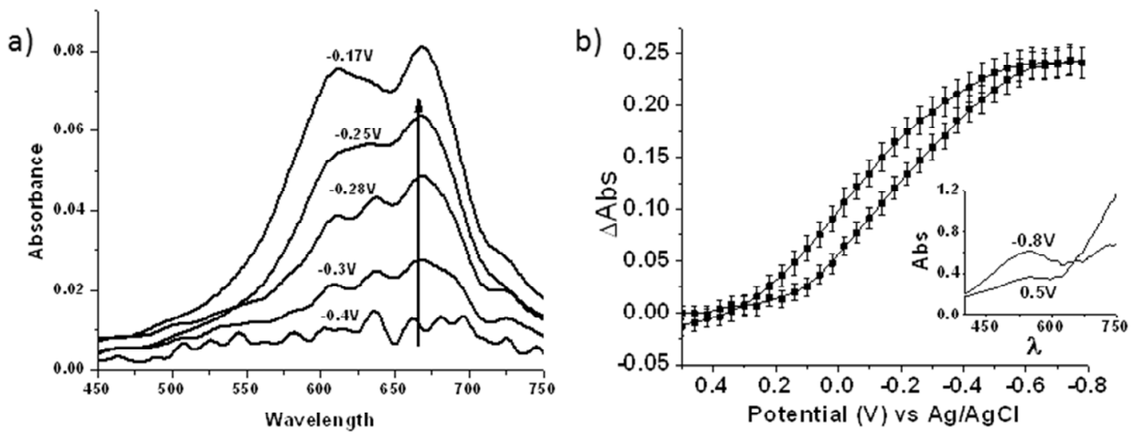

Fig. 5. Spectroelectrochemistry with the EA-FOC a) Potential dependent broadband absorbance spectra of an MB film and b) Absorbance difference (at 550 nm) verus potential for PEDOT film (inset: broadband absorbance spectra for reduced/oxidized polymer on the EA-FOC). Modified from Beam *et al.*, 2009.

The EA-FOC was used to electrochemically polymerize an ultra-thin film, estimated to be 0.3% of a monolayer, of poly (3,4-ethylenedioxythiophene) (PEDOT) and probe its electrochemical properties. The voltammogram of ultra-thin films of PEDOT has broad voltammetric peaks which are poorly distinquishable from the non-faradaic background.

However, PEDOT undergoes a reversible oxidation from the neutral dark blue form of the polymer to the almost transparent single polaron state and upon further oxidation the bipolaron state of the polymer. (Chen & Inganas, 1996) The spectroelectrochemical measurement in Figure 5b of the change in absorbance at the λ_{max} (550 nm) versus potential on the EA-FOC illustrates the electrochromic behavior of the polymer. The EA-FOC only monitors the appearance/disappearance of the dark blue neutral form of the polymer and does not indicate the state of the polymer upon oxidation. (Beam *et al.*, 2009) The EA-FOC has the requisite sensitivity to monitor optical redox changes in submonolayer surface coverages of molecular thin-films.

2. Fluorescence bioassay

Fluorescence detection architectures are of particular importance for biosensing applications where the fluorescence signal is detected against a zero background enabling low limits of detection, typically in the nano- to femto-molar range. Optical transducers have the advantages of being non-destructive, sensitive, and can be used for real-time and kinetic measurements. Fluorescence signal transduction has widespread applications due to the commercial availability of a variety of fluorescent labels which only require simple modification procedures for incorporation with biomolecules. Several reviews and books have been published which discuss the different fluorescent biosensor designs and applications. (Collings & Caruso, 1997; Cunningham, 1998; Janata *et al.*, 1994; Marazuela & Moreno-Bondi, 2002; Taitt *et al.*, 2005; Thompson, 2006)

Commonly biosensor architectures require immobilization of the biological recognition event onto a surface for which the evanescent field of optical waveguide platforms is specifically suited. Fiber-coupled sensor platforms do not require the bulky free-space optics used for fluorescence microscopy, total internal reflection fluorescence (TIRF), and planar waveguide techniques. Therefore, integrated excitation and emission fiber optic platforms have been constructed using different structures including a de-clad cylindrical core and tapered optical fibers. The FOC is the first demonstration of a multi-mode side polished fiber as a planar integrated excitation and emission platform.

2.1 Mechanism of back-coupled fluorescence

According to Snell's law, light traveling in a lower refractive index medium is refracted at a planar interface with angles below the critical angle in a high-index medium, such as a slab waveguide. For light to be guided within a waveguide it must be launched at angles greater than the critical angle; therefore, light from a lower refractive index medium cannot in principle be guided (Figure 6a). However, for surface confined fluorophores, the proximity of the fluorophores to the waveguiding structure allows coupling of the evanescent photons into guided modes of the waveguide termed back-coupled fluorescence. In other words, the electromagnetic near field, created by the oscillation of the excited dipole from the surface confined fluorophore, overlaps with the evanescent tail of the waveguide modes and meets the conditions for light propagation within the waveguide (Figure 6b). (Carniglia *et al.*, 1972) Harrick and Loeb first applied the principle of back-coupled fluorescence using an ATR element to detect a fluorescently labeled self-assembled thin-film of bovine serum albumin. Fiber optic based back-coupled fluorescence biosensors were first presented by Andrade *et al.* in 1985 and theoretically explored by Glass *et al.* and Marcuse.

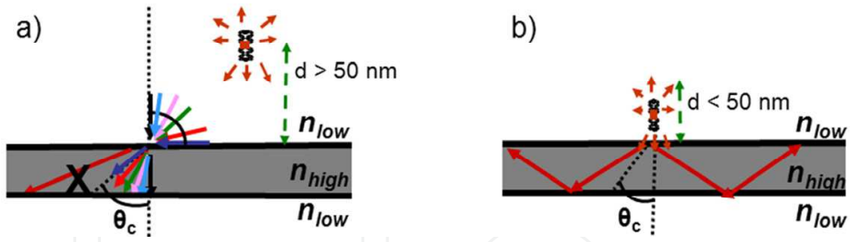

Fig. 6. Back-coupled fluorescence: a) light propagating from fluorophores far away from the waveguiding structure will be refracted at angles less than the critical angle, and therefore will not excite waveguide modes within the structure. b) Light propagating from fluorophores within close proximity of the waveguiding structure will back-couple fluorescence into the waveguide because the evanescent photons, or the near-field, of the fluorophore will overlap with the evanescent tail of propagating modes in the structure.

2.2 Fiber optic based fluorescence sensors

The pioneering research utilizing a de-clad quartz fiber to collect back-coupled fluorescence from immobilized biomolecules was presented by Sutherland *et.al*, Andrade *et.al*, and Glass *et.al*. Biosensors based on receptor proteins (Garden *et al.*, 2004; Rogers *et al.*, 1991; Rogers *et al.*, 1989), antibody-antigen interactions (Anis *et al.*, 1993; Bier *et al.*, 1992; Devine *et al.*, 1995; Eenink *et al.*, 1990; McCormack *et al.*, 1997; Oroszlan *et al.*, 1993; Shriver-Lake *et al.*, 1995; Toppozada *et al.*, 1997; Walczak *et al.*, 1992), sandwich immunoassay (Geng *et al.*, 2006; Kapoor *et al.*, 2004), and oligonucleotides (Abel *et al.*, 1996; Graham *et al.*, 1992; Pandey & Weetall, 1995) have been presented employing the de-clad fiber geometry. However, the de-clad fiber architecture is limited by the fragile nature of the fiber platform and inefficient fluorescence back-coupling due to the sharp V-number mismatch.

The V-number, or waveguide parameter, of a waveguide platform can be used to calculate the number of modes the structure will support (Equation 2).

$$V = \frac{2\pi r}{\lambda}\sqrt{\left(n_{core}^2 - n_{clad}^2\right)} \tag{2}$$

Where π and λ have their usual meanings, r is the radius of the fiber, n_{core} and n_{clad} are the refractive index of the core and cladding respectively. For example, a 50 µm fiber with an n_{core} of 1.460 and n_{clad} of 1.443 will have a V-number of 62 at 560 nm. For the de-clad fiber sensor geometry, the value of n_{clad} should be replaced with the aqueous medium surrounding the sensing platform (1.33); therefore, the V-number is 169 at 560 nm in the sensing region. Thus, approximately 60% of the modes in the sensing region of the fiber will not propagate in the fiber. To complicate the matter further, the back-coupled fluorescence primarily propagates in the higher order modes of the de-clad fiber, which are the non-propagating modes in the clad fiber.

One method researchers have employed to minimize back-coupled fluorescence loss due to V-number mismatch is to increase the value of n_{clad} in the sensing region of a de-clad fiber. Potyrailo and Hieftje have immobilized reagents sensitive to ammonia, humidity, and oxygen in the polymer cladding of optical fibers, thus ensuring no change in the value of n_{clad}. (Potyrailo & Hieftje, 1998; Potyrailo & Hieftje, 1999) An alternative strategy to increase n_{clad} in the sensing region of a de-clad fiber is the application of a sol-gel cladding containing an analyte sensitive dye. (Browne *et al.*, 1996; Kao *et al.*, 1998; MacCraith *et al.*, 1993; O'Keeffe

et al., 1995) A second method to match the V-number between the clad and unclad sensing region of fiber optic sensors is to decrease *r* in the sensing region through etching the de-clad fiber. Fluorescent fiber sensors, where the de-clad sensing region has been step- or taper-etched, exhibit a 20 to 50 fold improvement in sensitivity. (Anderson *et al.*, 1994; Anderson *et al.*, 1994) Tapered fiber optic biosensor platforms have been applied to sandwich assays (Golden *et al.*, 1992; Zhou *et al.*, 1997), immunosensors (Anderson *et al.*, 1993; Maragos & Thompson, 1999; Thompson & Maragos, 1996), and measuring pH. (Grant & Glass, 1997) The feasibility of collecting fluorescence using a single-mode biconical tapered fiber has also been explored. (Wiejata *et al.*, 2003)

The FOC provides a planar, robust, supported, side-polished multimode fiber platform for fluorescence biosensing applications. A related platform using a single-mode fiber in a bent configuration to collect the luminescence of a rhodamine 6-G film has been previously reported; however, this device was limited to single wavelength detection and relied on frequency modulated detection. (Poscio *et al.*, 1990) The ability to simply collect broadband fluorescence will enable the FOC device to be used in a broad range of sensor configurations using fluorescence detection systems, including on-chip, fully integrated excitation and sequential optical characterization of luminescent analytes. The first generation FOC device demonstrated back-coupled fluoresence with a drop cast film of CdSe semiconductor nanoparticles (SC-NP) as a luminescent model system. (Beam *et al.*, 2007) Here, the FOC is applied to quantitatively characterize a biotin-Streptavidin binding event as a model bioassay system.

2.3 BSA-biotin/streptavidin-CY bioassay on the planar fiber optic chip

A bioassay of surface-adsorbed biotin with fluorescently labeled streptavidin was chosen to quantitatively explore back-coupled fluorescence collection by the FOC. The small molecule biotin interacts non-covalently with the streptavidin protein and is highly specific, with one of the largest known binding constants ($K_a \cong 10^{15}$ M^{-1}). Bovine serum albumin (BSA) labeled with biotin (Sigma) adsorbs to the surface of the FOC and is transparent in the visible region. The back-coupled fluorescence is collected from the fluorescently labeled (Cascade Yellow, CY: Invitrogen) streptavidin bound to the surface adsorbed biotin. The Cascade Yellow dye was chosen for labeling due to its large Stokes shift (~150 nm) and short excitation wavelength. A fluorophore with a large Stokes shift is very valuable for back-coupled fluorescence measurements because of the magnified inner-filter effects of the fluorophores on the waveguide platform. Back-coupled fluorescence propagates in the waveguide modes; therefore, the emitted light is available in the evanescent field for re-absorption by the same film. The concentration dependence of the bioassay and the efficiency of the back-coupled fluorescence collected by the FOC are examined.

A representative spectrum of a BSA-biotin/streptavidin-CY film is plotted in Figure 7a along with two control experiments. The first control confirms that there is no contribution to the fluorescence from the BSA-biotin thin-film (blue line). The second control consisted of a BSA film, which was not labeled with biotin, to be incubated with the fluorescently tagged streptavidin to test for non-specific adsorption (green line). The contribution to the back-coupled fluorescence from non-specific adsorption of streptavidin-CY was shown to be below the detection limit of the experimental set-up. Finally, to confirm the back-coupled fluorescence resulted from the Cascade Yellow dye, the corrected back-coupled fluorescence spectrum is compared with the Cascade Yellow spectrum supplied by the manufacturer.

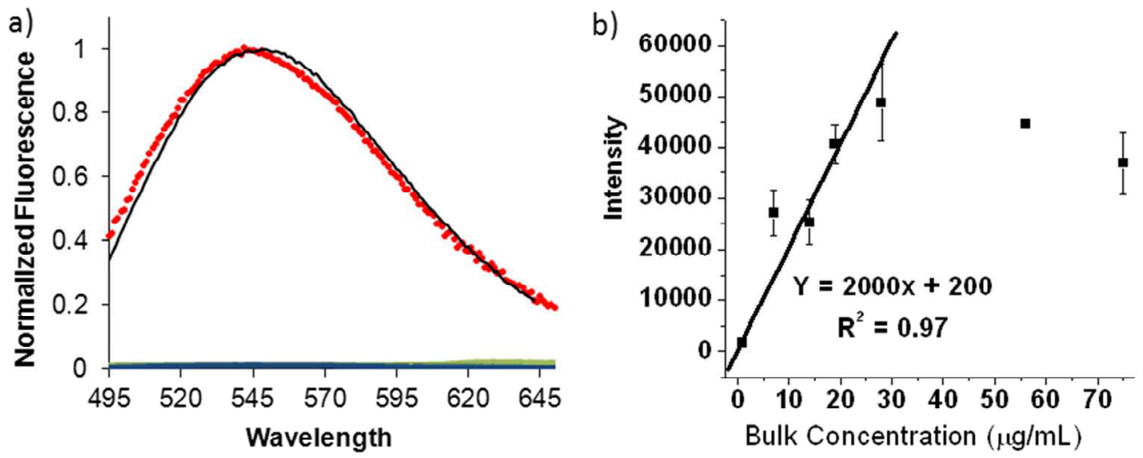

Fig. 7. Back-coupled fluorescence for a biotin/streptavidin bioassay. a) Cascade Yellow flourescence (black) spectra from the manufacturer (Invitrogen). Back-coupled fluorescence spectra for a BSA-biotin/streptavidin-CY film (red), background fluorescence from the buffer and biotin-BSA film was shown to be negligible (blue), and fluorescence due to nonspecific adsorption of the strepavidin was shown to be below the detection limit of the measurement (green) by using an unlabeled film of BSA. b) Bioassay calibration plot of the streptavidin-CY bulk concentration versus the average maximum collected fluorescence intensity on the FOC.

The concentration dependence of the collected back-coupled fluorescence for the bioassay was determined by varying the concentration of streptavidin-CY while maintaining the same adsorption conditions for the BSA-biotin film. The fluorescence for three BSA-biotin/streptavidin-CY films was collected for each bulk solution concentration (1, 7, 14, 19, 28, 56, and 75 μg/mL). A plot of bulk concentration versus the average fluorescence maximum intensity illustrates a linear dependence of fluorescence with bulk concentration and a R^2 value close to 0.97 for bulk concentrations less than 28 μM (Figure 7b). A self limiting surface coverage at bulk concentrations ≥ 28 μM was observed. The subsequent slight decline in fluorescence for the higher bulk concentrations is attributed to luminescence quenching and photobleaching of dyes in close proximity to each other. The observed bulk concentration limit of detection for the biotin/streptavidin bioassay is 15 nM, which is on the order of the LOD reported for several de-clad fiber fluorescence sensors. (Anis *et al.*, 1993; Devine *et al.*, 1995; Eenink *et al.*, 1990; Graham *et al.*, 1992; McCormack *et al.*, 1997; Oroszlan *et al.*, 1993; Pandey & Weetall, 1995; Shriver-Lake *et al.*, 1995; Sutherland *et al.*, 1984) However, the measured pathlength of the FOC is only ~ 24 mm for this device compared to the ~ 60 mm pathlength of most cylindrical core de-clad fiber sensor platforms. The de-clad fiber sensor platforms require large fiber cores (~ 600 μm) with low modal surface interaction to increase mechanical strength, and therefore, a long interaction length is necessary. The supported planar substrate of the side polished FOC increases the mechanical robustness of the platform; thus, smaller core (50 μm), more surface sensitive fibers are used. One method which could be employed to decrease the LOD of the FOC based fluorescence sensor, and to surpass the de-clad fiber platforms, is to increase the physical pathlength of the FOC device.

2.4 Back-coupled fluorescence collection efficiency

To quantify the fluorescence collection of the FOC using the BSA-biotin/streptavidin-CY bioassay an efficiency calculation was conducted. The backcoupled fluorescence collection efficiency is calculated from the power ratio of the actual fluorescence collected (P_{FOC}) and the calculated total power of fluorescence of the film (P_{calc}) (Equation 3).

$$Efficiency = \frac{P_{FOC}}{P_{calc}} = \frac{P_{FOC}}{P_o L\left(1-10^{-A_{405}}\right)Q_{cy}} \tag{3}$$

P_{FOC} is the area under a gaussian fit curve to the corrected fluorescence spectrum detected (mW). The values in the denominator are an expression of the calculated fluorescence power propagating in all directions, where P_o is the power launched into the fiber from the 405 nm laser (mW); L is defined as 1-Loss of the FOC; $\left(1-10^{-A_{405}}\right)$ is the percent of power absorbed at 405 nm by the dye and available to be converted to fluorescence; and Q_{cy} is the quantum yield of the Cascade Yellow labeled streptavidin. The calculated back-coupled fluorescence efficiency is 0.02% of the light emitted by the Cascade Yellow dye. For comparison, only 2% of the light emitted from an isotropic emitter is typically collected with a lens. To improve device performance and decrease the detection, the FOC should be engineered to more efficiently collect back-coupled fluorescence. The back-coupled fluorescence efficiency could be improved upon by increasing the numerical aperture/refractive index of the fiber; however, the extent of V-number mismatch of the FOC platform should be evaluated in conjunction with alternative FOC architectures.

3. Bright and broadband-guided light source

Field portable optical sensing devices require light sources that are robust, compact, spectrally broad, and bright. The ideal fiber coupled light source will have high power per unit area and unit solid angle; thus, yielding high power per guided mode inside an optical fiber. Using the back-coupled light mechanism of fluorescent thin-films deposited on the FOC platform, a fully integreated broadband, bright guided light source is created. The FOC light source is produced by pumping an aluminum tris-hydroxyquinoline thin-film capped with a silicon dioxide overlayer. A directly fiber coupled broadband FOC source extending from 405 nm to 650 nm is produced with an output of 1.8 mW, which is significantly brighter than a fiber-coupled tungsten source and spectrally borader than a light emitting diode (LED) source.

3.1 Fiber optic light sources

Bright and spectrally broad light sources are currently required for several applications including optical coherence tomography, optical spectroscopies, and chemical/biological sensing. Recently, several promising technologies have been developed to fulfill those needs. In particular, superluminescent LEDs (Zhang *et al.*, 2009), supercontinuum-generation light sources (Berge *et al.*, 2007), and amplified spontaneous emission (Samuel & Turnbull, 2007) are becoming increasingly useful for many applications. Despite those developments, a cost-effective light source that is fiber-coupled, spectrally broad, and bright is still in quite demand, especially in the visible and ultra-violet regions of the spectrum.

3.2 Planar fiber optic chip broadband light source

The planar geometry of the FOC device is amenable to standard thin-film deposition architectures such as thermal deposition. The back-coupled fluorescence from an organic fluorophore deposited on the polished surface of the FOC platform is used to create a fully integrated fiber optic broadband light source. With the growing interest in organic LEDs and photovoltaic devices, a vast number of inexpensive, easily processable, high quantum yield fluorescent organic materials are commercially available. (Kafafi, 2005; Li *et al.*, 2007) These fluorescent organic compounds garner much interest because of their broad emission spectrum when compared to inorganic compounds such as GaN and Si. Tris-aluminum 8-hydroxyquinoline (Alq3) was chosen as a fluorescent material for the FOC light source due to its broad emission in the visible region. A 45 nm thick film of Alq3 was deposited on the FOC using thermal deposition. Both oxygen and water can cause degradation of the Alq3 thin-film (Burrows *et al.*, 1994; McElvain *et al.*, 1996); therefore, FOC light source devices must be protected from the ambient environment to ensure continued operation. Encapsulation of the FOC device was achieved with a 100 nm film of SiO_2 deposited, by electron beam evaporation, over the Alq3 film without breaking vacuum. Emission of the Alq3 film on the FOC device is achieved with pumping the film with a 405 nm GaN laser diode which is fiber coupled into the FOC platform. Figure 8a shows a picture of the active region of the FOC light source, where luminescence in the Alq3 film is back-coupled into guided modes of the fiber, next to the light out-coupled from the FOC fiber.

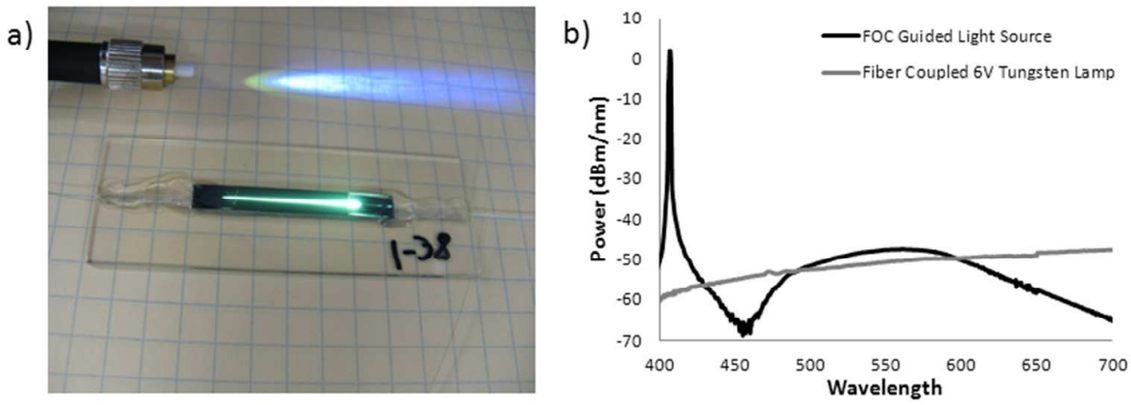

Fig. 8. a) Image of the FOC light source device; b) comparison of the fiber output of the FOC light source with a fiber coupled 6V tungsten-halogen lamp.

A comparison of the out-coupled spectrum from the FOC light source with a fiber coupled 6V tungsten lamp are plotted in Figure 8b. The light from the thermal source (6V tungsten lamp) is coupled into the same patch cable as the FOC using similar high precision aspheric optics. The fluorescence from the FOC light source has an increased out-coupled intensity over a 100 nm range from 480 to 580 nm overlapping with the Alq3 emission peak compared to the fiber coupled thermal source. The spectra resulting from the FOC light source includes a large intensity peak at 405 nm for the laser used to pump the film. The measured power intensity out-coupled from the FOC light source was measured to be 1.8 mW.

While optical pumping was used for these experiments, there is the potential to use an electrically pumped system to directly drive the FOC light source producing broadband

spectra with high brightness. Using an ITO film as a transparent electrode, organic layers could be built onto the FOC structure very similar to that of an organic light emitting diode. Combining emission spectra for multiple organic films would allow an even broader output spectrum to be achieved. With the amount of research in organic fluorescent compounds with increased quantum efficiences and variety of wavelength ranges, improving the power output and wavelength range of future FOC light source devices will be developed.

4. Raman spectroscopy

Raman spectroscopy is a well-established analytical technique that can identify chemical and physical properties through interactions with the vibrational states of a particular analyte. This section presents investigations of excitation and collection of Raman scattering using the FOC for thin molecular films. Thin-film Raman measurements were achieved with the added signal enhancement of surface enhanced raman spectroscopy (SERS). Gold nanoparticles are deposited on the FOC surface to enhance the Raman signal of a 4-aminothiophenol film and the Raman signal was both excited and collected by the FOC in decoupled instrument schemes. In a similar approach, Raman scattering of carbon nanotubes was demonstrated, setting the stage for the FOC as a platform for interesting chemical analysis.

4.1 Raman scattering

Raman spectroscopy relies on the inelastic scattering of incident light with Raman active molecular thin-films. Typically, in an elastic event known as Rayleigh scattering, the excited molecule relaxes back to the initial ground state and light of equal energy to the incident light is reemitted. Raman scattering occurs when interactions between molecular vibrations and rotations with the incident light result in lower frequency, Stokes, or higher frequency, anti-Stokes, shifts from the incident frequency of light. Raman spectra are independent of the initial frequency of the incident light, and the resultant energy spectrum is a signature of the vibrational/rotational states of the probed molecules.

Raman scattering occurs for only one out of every 10^6-10^8 scattering events, making it a very weak signal. (Smith & Dent, 2005) To improve upon this small cross section, researchers have utilized the effects of localized surface plasmon resonance. A localized surface plasmon resonance occurs when small metallic structures are irradiated by light. Similar to a lightning rod, these structures induce an electric-field enhancing corona effect. This effect relies on the size of the metallic structure to be small compared to the wavelength of the incident light, and the electric-field will concentrate in areas of greatest curvature. Surface enhanced Raman spectroscopy (SERS) occurs when Raman active molecules are in the presence of roughened metallic surfaces or nanoparticles. The electric-field amplitude will generate a larger intensity of the incident light as well as amplify Raman scattering. The SERS amplification effect has lead to reported Raman signal enhancements of 10^6 (Felidj *et al.*, 2003), 10^{11} (Gupta & Weimer, 2003), even 10^{14} (Kneipp *et al.*, 1997). (Willets & Van Duyne, 2007)

Increasing Raman spectroscopy sensitivity has been sought after in recent years, ultimately reaching single molecule detection. (Kneipp *et al.*, 1997; Xu *et al.*, 1999) Particularly, thin-film characterization is of interest to a growing number of fields yet analysis by conventional commercial Raman microscope instruments is difficult due to the convolution between analyte and substrate Raman activity. The unique geometry of the FOC allows for analyzing

a strip of sample rather than a single spot as found in conventional Raman machine. We present here the extended ability of the FOC to both excite and collect Raman scattering of thin-films.

4.2 Fiber optic raman probes

The use of distal end fiber probes for Raman scattering has been ongoing for some time. Although mechanisms have been described for propagating the excitation beam and collected Raman scattering through a single fiber (Potyrailo *et al.*, 1998), these devices often utilize separate launching and collection fibers. In some schemes, a single launching fiber is surrounded by a bundle of collection fibers. Raman spectroscopy using distal end fiber probes has been demonstrated in a number of chemical (Khijwania *et al.*, 2007; McCreery *et al.*, 1983; Tiwari *et al.*, 2007) and biomedical (Krafft *et al.*, 2007; Lima *et al.*, 2008; Vo-Dinh *et al.*, 1999) applications. However, the overlap between the illumination cone and the collection cone is often poor for these sensor platforms, weakening the already very faint Raman signal. To improve sensitivity of Raman sensors modifications such as GRIN lens application to the distal end (Mo *et al.*, 2009) or tapered fibers (Stokes et al., 2004) have been implemented. Although these changes have shown some improvement in overall signal to noise ratio, the move to a planar fiber optic chip offers the advantages of simplifying optical alignment and providing a larger surface area for interaction.

Exposing the core of the optical probe allows for the use of evanescent field interactions of the exposed fiber core with immobilized analytes. Here the fiber core may be functionalized to capture the analyte or to enhance the Raman signal as in the case of a SERS substrate. In a D-shaped device similar to the FOC, Zhang *et al.* were able to demonstrate the excitation of the Raman analyte Rhodamine 6G by a SERS functionalized planar probe (Zhang *et al.*, 2005). Near-field interactions do not rely on the optical alignment of the system; therefore, a more streamlined approach would only use a single fiber for both excitation and collection of the Raman signal. Coupled excitation and collection of SERS for an exposed core fiber has been demonstrated for thin-film and aqueous samples (Stokes & Vo-Dinh, 2000); however, the exposed fragile core limits the applications of this sensor architecture.

4.3 Raman spectroscopy with the FOC

A single fiber is used to deliver the excitation beam and collect the scattered Raman signal to form a fully integrated system. At the boundary of the exposed core of the FOC, adsorbed analytes interact with the evanescent field of the excitation light. The Raman signal of the analyte may then be launched into the fiber through near-field coupling. To test the FOC for its function in Raman spectroscopy, the excitation and collection of the Raman signal was decoupled. In the excitation scheme, laser light (632.8 nm) was launched into the fiber and the adsorbed analyte was excited. The scattered Raman signal was then collected by external optical components mounted over the FOC and delivered to a spectrometer connected to a CCD for data acquisition. For the collection scheme, external optics were used to deliver the excitation laser beam to the planar surface of the FOC. The Raman signal was then coupled into the FOC and guided by the fiber to the data acquisition set-up. Since, in both schemes, Rayleigh scattering of the laser line was generated, a notch filter was placed in the beam path before the spectrometer to remove as much of the initial laser beam as possible. Both schemes are shown in Figure 9.

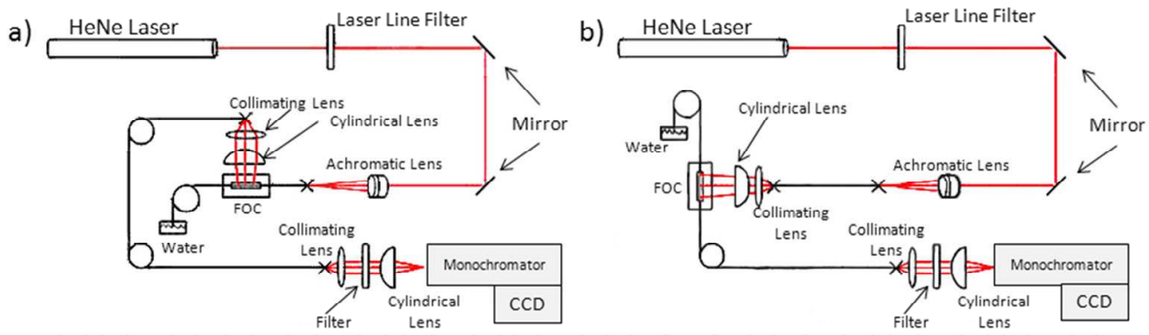

Fig. 9. The experimental set-up for the a) excitation scheme in which the light is delivered to the analyte by evanescent waves, and the b) collection scheme in which the light is directly focused on the FOC surface.

As a proof of concept study, the FOC was tested in the excitation scheme for the generation of Raman scattering of bulk media. A commercial optical gel (Cargille) was chosen for its potential as a higher index capping media for thin-films. The gel was deposited in a thin, even layer across the active area of the FOC. The Raman signal of the gel was induced by the FOC and collected by the external optics as seen in Figure 10. Demonstrating the feasibility of Raman excitation by the FOC sets the stage for the chip to be employed in other bulk media investigations without the need for surface enhancement. However, the more interesting objective was to determine the utility of the FOC in generating Raman scattering of smaller volumes of analyte such as in the case of thin-films.

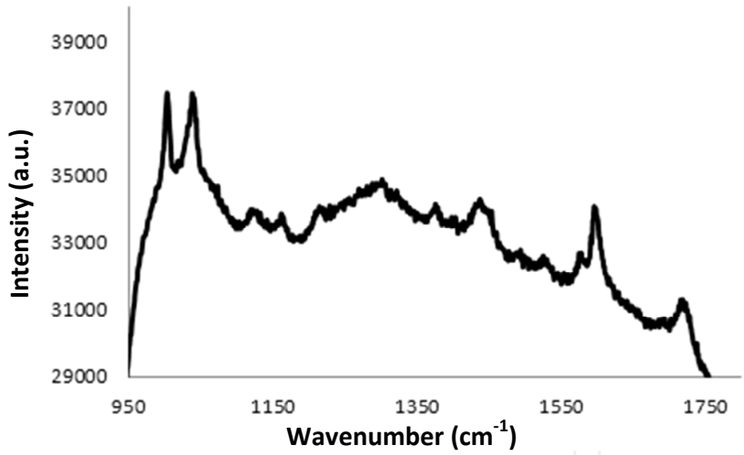

Fig. 10. Raman scattering of commericially available optical gel excited by the FOC.

4.4 Surface enhanced raman of thin films with the FOC

For thin-film analysis, the FOC was first functionalized with gold nanoparticles to create a SERS substrate. A seed based method (Wei *et al.*, 2004; Wei & Zamborini, 2004) was performed directly on the FOC platform. In short, the process required three stages. First, the FOC was functionalized with 3- mercaptopropyltrimethoxysilane (MPTMS). Next, 5 nm gold nanoparticles were adsorbed to the MPTMS functionalized FOC platform. Finally, a gold growth solution catalyzed the growth of the nanoparticles to rods, platelets, and spheroids on the order of 20 nm in diameter.

The first analyte investigated was 4-aminothiophenol (p-ATP). Raman activity of p-ATP in the presence of gold SERS substrates has been well documented. (Baia *et al.*, 2006; Guo *et al.*, 2007; Wang *et al.*, 2008) The analyte was deposited onto the FOC by submersion in an ethanol solution overnight. The FOC was washed and dried under a nitrogen flow before analysis of the thin-film. As shown in Figure 11a, the Raman signal of p-ATP was excited by the FOC and collected by external optics in the excitation scheme. Similar results were achieved by external excitation of the analyte and collection of the Raman signal via the FOC in the Collection Scheme. Both spectra are consistent with published data of p-ATP Raman activity as well as spectra of the p-ATP coated FOC collected by a commercial machine (Renishaw Invia). To attain acceptable signal-to-noise ratios, integration times of 5 to 10 minutes were used. Signal was detected for sub mW incident laser power, suggesting a low power light source could be used in a field version of the FOC Raman sensor platform.

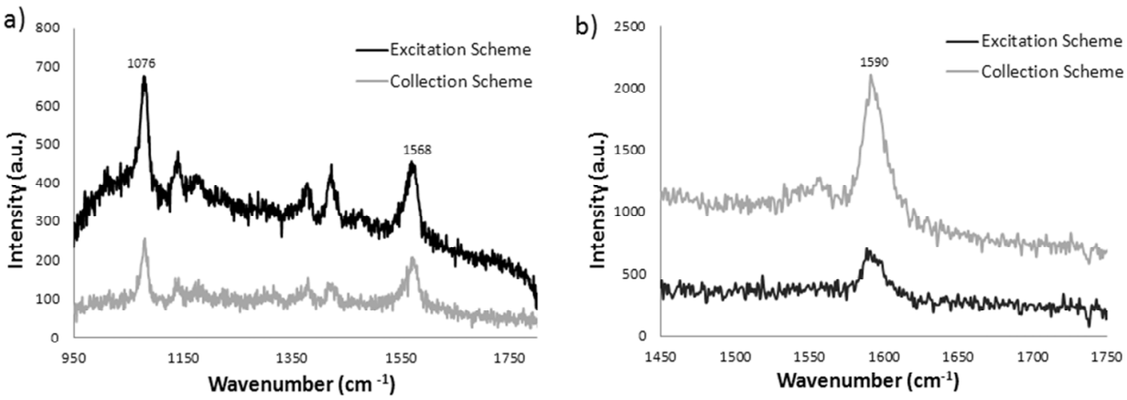

Fig. 11. a) Raman spectroscopy of p-ATP using both the excitation and collection schemes on the FOC. b) Excitation and collection of CNT G-band Raman signal by the FOC.

The second analyte studied with the Raman FOC device coated with gold nanoparticles was carbon nanotubes (CNT) in an isopropanol solution. In this case, the CNT were deposited by a drop cast method and remained in solution during analysis. The G-band of the CNT spectra was examined in both the excitation and collection schemes using the FOC. The data, shown in Figure 11b, was consistent with established Raman data for the CNT G-band. (Dresselhaus *et al.*, 2005; Kneipp *et al.*, 2004) Pairing the FOC device with the specific and nondestructive technique of Raman spectroscopy is a very desirable application.

5. Conclusion

In this chapter the current applications of the FOC platform were presented. FOC fabrication consists of an optical fiber mounted in a V-groove block, side-polished to create a planar platform that allows access to the evanescent field escaping from the fiber core. Currently, the FOC yields thin-film abosrbance sensitivity comparable with existing ATR instrumentation; however, it eliminates the complex coupling optics and alignment procedures used with planar waveguide based instrumentation. Spectroelectrochemical measurements on an ITO coated FOC platform have been previously demonstrated for both the potential dependent spectra of a methylene blue film and 0.3% of a monolayer of a conductive polymer film. Additionally, light generated in a surface-confined thin molecular

film can be back-coupled into the FOC platform when the conditions for light propagation within the waveguide are met. Back-coupled light into the FOC was used for the first time here to expand the applications of the FOC platform to a fluorescence bioassay, a broadband fiber optic light source, and Raman interrogation of molecular adsorbates. A BSA-biotin/streptavidin-CY fluorescence bioassay was demonstrated on the FOC with a limit-of-detection of 15 nM and calculated back-coupled fluorescence efficiency of 0.02%. A 1.8 mW directly fiber coupled broadband FOC source extending from 405 nm to 650 nm is produced with a SiO_2 capped Alq3 film deposited on the FOC, which is significantly brighter than a fiber-coupled tungsten source and spectrally broader than a LED source. Finally the FOC platform was modified with gold nanoparticles to create a surface enhanced Raman substrate for detection of 4-aminothiophenol and carbon nanotubes. Contrary to the un-clad fiber approach, the FOC with a supported planar interface can facilitate the use of conventional planar deposition technologies and provide a robust planar platform that is amenable for integration into various sensor applications.

6. Acknowledgments

This work was supported by the National Science Foundation under grants Number DBI-0352449, CTS-0428885, CHE-0517963, and CHE-0515963, the Kentucky Science and Technology Corporation under grant KSEF-1869-RDE-012, and the Science and Technology Center-Materials and Devices for Information Technology Research Grant Number DMR-0120967. B.M.B. acknowledges fellowship support from a TRIF Proposition 301 (Arizona) Graduate Fellowship in Photonics. The authors would like to thank Neal R. Armstrong, Jill Craven, Jinuk Jang, Yevgeniy Merzlyak, Gary Paysnoe, Clayton Shallcross, and Joseph Lynch for their scientific contributions to this work.

7. References

Abel, A. P., M. G. Weller, et al. (1996). Fiber-Optic Evanescent Wave Biosensor for the Detection of Oligonucleotides. *Analytical Chemistry*, Vol. 68, pp. 2905-2912

Anderson, G. P., J. P. Golden, et al. (1993). A Fiber Optic Biosensor: Combination Tapered Fibers Designed for Improved Signal Acquisition. *Biosensors and Bioelectronics*, Vol. 8, 5, pp. 249-256

Anderson, G. P., J. P. Golden, et al. (1994). An Evanescent Wave Biosensor-Part 2: Fluorescent Signal Acquisition from Tapered Fiber Optic Probes. *IEEE Transactions on Biomedical Engineering*, Vol. 41, 6, pp. 585-591

Anderson, G. P., J. P. Golden, et al. (1994). An Evanescent Wave Biosensor-Part I: Fluorescent Signal Acquisition from Step-Etched Fiber Optic Probes. *IEEE Transactions on Biomedical Engineering*, Vol. 41, 6, pp. 578-584

Andrade, J. D., R. A. Vanwagenen, et al. (1985). Remote Fiber-Optic Biosensors Based on Evanescent-Excited Fluoro-Immunoassay: Concept and Progress. *IEEE Transactions on Electron Devices*, Vol. ED-32, 7, pp. 1175-1179

Anis, N. A., M. E. Eldefrawi, et al. (1993). Reusable Fiber Optic Immunosensor for Rapid Detection of Imazethapry Herbicide. *Journal of Agricultural and Food Chemistry*, Vol. 41, pp. 843-848

Baia, M., F. Toderas, et al. (2006). Probing the enhancement mechanisms of SERS with p-aminothiophenol molecules adsorbed on self-assembled gold colloidal nanoparticles. *Chemical Physics Letters*, Vol. 422, 1-3, pp. 127-132

Bariain, C., I. R. Matias, et al. (2000). Optical Fiber Humidity Sensor Based on a Tapered Fiber Coated with Agarose Gel. *Sensors and Actuators B*, Vol. 69, pp. 127-131

Beam, B. M., N. R. Armstrong, et al. (2009). An Electroactive Fiber Optic Chip for Spectroelectrochemical Characterization of Ultra-Thin Redox Active Films. *Analyst*, Vol. 134, pp. 454-459

Beam, B. M., R. C. Shallcross, et al. (2007). Planar Fiber-Optic Chips for Broadband Spectroscopic Interrogation of Thin-Films. *Applied Spectroscopy*, Vol. 61, 6, pp. 585-592

Berge, L., S. Skupin, et al. (2007). Ultrashort filaments of Light in Weakly Ionized, Optically Transparent Media. *Reports on Progress in Physics*, Vol. 70, pp. 1633-1713

Bergmann, K. and C. T. O'Konski. (1963). A Spectroscopic Study of Methylene Blue Monomer, Dimer and Complexes with Montmorillonite. *Nature*, Vol. 67, pp. 2169-2177

Bier, F. F., W. Stocklein, et al. (1992). Use of a fibre optic immunosensor for the detection of pesticides. *Sensors and Actuators B*, Vol. 7, pp. 509-512

Blair, D. S., L. W. Burgess, et al. (1997). Evanescent Fiber-Optic Chemical Sensor for Monitoring Volatile Organic Compounds in Water. *Analytical Chemistry*, Vol. 69, pp. 2238-2246

Bradshaw, J. T., S. B. Mendes, et al. (2003). Broadband Coupling into a Single-Mode, Electroactive Integrated Optical Waveguide for Spectroelectrochemical Analysis of Surface-Confined Redox Couples. *Analytical Chemistry*, Vol. 75, 5, pp. 1080-1088

Bradshaw, J. T., S. B. Mendes, et al. (2005). Planar Integrated Optical Waveguide Spectroscopy. *Analytical Chemistry*, Vol. 77, 1, pp. 29A-36A

Browne, C. A., D. H. Tarrant, et al. (1996). Intrinsic Sol-Gel Clad Fiber-Optic Sensors with Time-Resolved Detection. *Analytical Chemistry*, Vol. 68, 14, pp. 2289-2295

Burrows, P. E., V. Bulovic, et al. (1994). Reliability and Degredation of Organic Light Emitting Devices. *Applied Physics Letters*, Vol. 65, pp. 2922-2924

Carniglia, C. K., L. Mandel, et al. (1972). Absorption and Emission of Evanescent Photons. *Journal of the Optical Society of America*, Vol. 62, 4, pp. 479-486

Chen, X. and O. Inganas. (1996). Three-Step Redox in Polythiophenes: Evidence from Electrocheistry at an Ultramicroelectrode. *Journal of Physical Chemistry*, Vol. 100, pp. 15202-15206

Collings, A. F. and F. Caruso. (1997). Biosensors: Recent Advances. *Reports on Progress in Physics*, Vol. 60, pp. 1397-1445

Cunningham, A. J. (1998). *Introduction to Bioanalytical Sensors* John Wiley and Sons, Inc., New York

Devine, P., N. A. Anis, et al. (1995). A Fiber-Optic Cocaine Biosensor. *Analytical Biochemistry*, Vol. 227, pp. 216-224

Diaz-Herrera, N., M. C. Navarrete, et al. (2004). A Fibre-Optic Temperature Sensor Based on the Deposition of a Thermochromic Material on an Adiabatic Taper. *Measurement Science and Technology*, Vol. 15, pp. 353-358

Doherty, W. J., C. L. Donley, et al. (2002). Broadband Spectroelectrochemical Attenuated Total Reflectance Instrument for Molecular Adlayer Studies. *Applied Spectroscopy*, Vol. 56, 7, pp. 920

Doherty, W. J., A. G. Simmonds, et al. (2005). Molecular Ordering in Monolayers of an Alkyl-Substituted Perylene-Bisimide Dye by Attenuated Total Reflectance Ultraviolet-Visible Spectroscopy. *Applied Spectroscopy*, Vol. 59, 10, pp. 1248-1256

Dresselhaus, M. S., G. Dresselhaus, et al. (2005). Raman spectroscopy of carbon nanotubes. *Physics Reports-Review Section of Physics Letters*, Vol. 409, 2, pp. 47-99

Dunphy, D. R., S. B. Mendes, et al. (1997). The Electroactive Integrated Optical Waveguide: Ultrasensitive Spectroelectrochemistry of Submonolayer Adsorbates. *Analytical Chemistry*, Vol. 69, 15, pp. 3086-3094

Dunphy, D. R., S. B. Mendes, et al. (1999). Spectroelectrochemistry of Monolayer and Submonolayer Films Using an Electroactive Integrated Optical Waveguide. In: *Interfacial Electrochemistry: Theory, Experiment and Applications*. A. Wieckowski. pp. (513-525), Marcel Dekker, Inc., New York

Eenink, R. G., H. E. de Bruijn, et al. (1990). Fibre-Fluorescence Immunosensor Based on Evanescent Wave Detection. *Analytica Chimica Acta*, Vol. 238, pp. 317-321

Egami, C., K. Takeda, et al. (1996). Evanescent-Wave Spectroscopic Fiber Optic pH Sensor. *Optics Communications*, Vol. 122, pp. 122-126

Felidj, N., J. Aubard, et al. (2003). Optimized surface-enhanced Raman scattering on gold nanoparticle arrays. *Applied Physics Letters*, Vol. 82, 18, pp. 3095-3097

Flora, W. H., S. B. Mendes, et al. (2005). Determination of Molecular Anisotropy in Thin Films of Discotic Assemblies Using Attenuated Total Reflectance UV -Visible Spectroscopy. *Langmuir*, Vol. 21, 1, pp. 360-368

Garden, S. R., G. J. Doellgast, et al. (2004). A Fluorescent Coagulation Assay for Thrombin Using a Fiber Optic Evanescent Wave Sensor. *Biosensors and Bioelectronics*, Vol. 19, pp. 737-740

Geng, T., J. Uknalis, et al. (2006). Fiber-Optic Biosensor Employing Alexa-Fluor Conjugated Antibody for Detection of *Escherichia coli* O157:H7 from Ground Beef in Four Hours. *Sensors*, Vol. 6, pp. 796-807

Glass, T. R., S. Lackie, et al. (1987). Effect of Numerical Aperture on Signal Level in Cylindrical Waveguide Evanescent Fluorosensors. *Applied Optics*, Vol. 26, 11, pp. 2181-2187

Gloge, D. (1971). Weakly Guiding Fibers. *Applied Optics*, Vol. 10, 10, pp. 2252-2258

Golden, J. P., L. C. Shriver-Lake, et al. (1992). Fluorometer and Tapered Fiber Optic Probes for Sensing in the Evanescent Wave. *Optical Engineering*, Vol. 31, 7, pp. 1458-1462

Graham, C. R., D. Leslie, et al. (1992). Gene Probe Assays on a Fibre-Optic Evanescent Wave Biosensor. *Biosensors and Bioelectronics*, Vol. 7, pp. 487-493

Grant, S. A. and R. S. Glass. (1997). A Sol-Gel Based Fiber Optic Sensor for Local Blood pH Measurements. *Sensors and Actuators B*, Vol. 45, pp. 35-42

Green, N. M. (1975). *Advances in Protein Chemistry*, Vol. 29, pp. 85-133

Guo, S. and S. Albin. (2003). Transmission Properties and Evanescent Wave Absorption of Cladded Multimode Fiber Tapers. *Optics Express*, Vol. 11, 3, pp. 215-223

Guo, S. J., Y. L. Wang, et al. (2007). Large-scale, rapid synthesis and application in surface-enhanced Raman spectroscopy of sub-micrometer polyhedral gold nanocrystals. *Nanotechnology*, Vol. 18, 40,

Gupta, B. D. and Ratnanjali. (2001). A Novel Probe for a Fiber Optic Humidity Sensor. *Sensors and Actuators B*, Vol. 80, pp. 132-135

Gupta, B. D. and D. K. Sharma. (1997). Evanescent Wave Absorption Based Fiber Optic pH Sensor Prepared by Dye Doped Sol-Gel Immobilization Technique. *Optics Communications*, Vol. 140, pp. 32-35

Gupta, B. D. and N. K. Sharma. (2002). Fabrication and Characterization of U-Shaped Fiber-Optic pH Probes. *Sensors and Actuators B*, Vol. 82, pp. 89-93

Gupta, B. D., C. D. Singh, et al. (1994). Fiber Optic Evanescent Field Absorption Sensor: Effect of Launching Condition and the Geometry of the Sensing Region. *Optical Engineering*, Vol. 33, 6, pp. 1864-1868

Gupta, R. and W. A. Weimer. (2003). High enhancement factor gold films for surface enhanced Raman spectroscopy. *Chemical Physics Letters*, Vol. 374, 3-4, pp. 302-306

Harrick, N. J. and G. I. Loeb. (1973). Multiple Internal Reflection Fluroescence Spectrometry. *Analytical Chemistry*, Vol. 45, 4, pp. 687-691

Hartnagel, H. L., A. L. Dawar, et al. (1995). *Semiconducting Transparent Thin Films* Institute of Physics Publishing, Philadelphia

Invitrogen. (2007). Spectra-Cascade Yellow Goat Anti-Mouse IgG Antibody/pH 8.0, Available from: <http://probes.invitrogen.com/servlets/spectra?fileid=10995ph8>

Itoh, K. and A. Fujishima. (1988). An Application of Optical Waveguides to Electrochemistry: Construction of Optical Waveguide Electrodes. *Journal of Physical Chemistry*, Vol. 92, pp. 7043-7045

Janata, J., M. Josowicz, et al. (1994). Chemical Sensors. *Analytical Chemistry*, Vol. 66, pp. 207R-228R

Kafafi, Z. H. (2005). *Organic Electroluminescence* Taylor & Francis Group, Boca Raton, FL

Kao, H. P., N. Yang, et al. (1998). Enhancement of Evanescent Fluorescence from Fiber-Optic Sensors by Thin-Film Sol-Gel Coatings. *Journal of the Optical Society of America A*, Vol. 15, 8, pp. 2163-2171

Kapoor, R., N. Kaur, et al. (2004). Detection of Trophic Factor Activated Signaling Molecules in Cells by a Compact Fiber-Optic Sensor. *Biosensors and Bioelectronics*, Vol. 20, pp. 345-349

Kendall, D. L. (1979). Vertical Etching of Silicon at Very High Aspect Ratios. *Annual Review of Material Science*, Vol. 9, pp. 373-403

Khijwania, S. K. and B. D. Gupta. (1998). Fiber Optic Evanescent Field Absorption Sensor with High Sensitivity and Linear Dynamic Range. *Optics Communications*, Vol. 152, pp. 259-262

Khijwania, S. K. and B. D. Gupta. (2000). Maximum Achievable Sensitivity of the Fiber Optic Evanescent Field Absorption Sensor Based on the U-Shaped Probe. *Optics Communications*, Vol. 175, pp. 135-137

Khijwania, S. K., V. S. Tiwari, et al. (2007). A fiber optic Raman sensor for hydrocarbon detection. *Sensors and Actuators B-Chemical*, Vol. 125, 2, pp. 563-568

Kneipp, K., H. Kneipp, et al. (2004). Surface-enhanced Raman scattering on single-wall carbon nanotubes. *Philosophical Transactions of the Royal Society of London Series a-Mathematical Physical and Engineering Sciences*, Vol. 362, 1824, pp. 2361-2373

Kneipp, K., Y. Wang, et al. (1997). Single molecule detection using surface-enhanced Raman scattering (SERS). *Physical Review Letters*, Vol. 78, 9, pp. 1667-1670

Krafft, C., M. Kirsch, et al. (2007). Methodology for fiber-optic Raman mapping and FTIR imaging of metastases in mouse brains. *Analytical and Bioanalytical Chemistry*, Vol. 389, 4, pp. 1133-1142

Kuswandi, B., R. Andres, et al. (2001). Optical Fibre Biosensors Based on Immobilized Enzymes. *The Analyst*, Vol. 126, pp. 1469-1491

Leung, A., P. M. Shankar, et al. (2007). Real-Time Monitoring of Bovine Serum Albumin at Femtogram/mL Levels on Antibody-Immobilized Tapered Fibers. *Sensors and Actuators B*, Vol. 123, pp. 888-895

Leung, A., P. M. Shankar, et al. (2007). A Review of Fiber-Optic Biosensors. *Sensors and Actuators B*, Vol. 125, pp. 688-703

Li, Z., Z. R. Li, et al. (2007). *Organic Light-Emitting Materials and Devices* CRC Press Taylor & Francis Group, Boca Raton

Lima, C. J., M. T. T. Pacheco, et al. (2008). Catheter with dielectric optical filter deposited upon the fiber optic end for Raman in vivo biospectroscopy applications. *Spectroscopy-an International Journal*, Vol. 22, 6, pp. 459-466

MacCraith, B. D. (1993). Enhanced Evanescent Wave Sensors Based on Sol-Gel Derived Porous Glass Coatings. *Sensors and Actuators B*, Vol. 11, pp. 29-34

MacCraith, B. D., C. M. McDonagh, et al. (1993). Fibre Optic Oxygen Sensor Based on Fluroescence Quenching of Evanescent-Wave Excited Ruthenium Complexes in Sol-Gel Derived Porous Coatings. *Analyst*, Vol. 118, pp. 385-388

Mackenzie, H. S. and F. P. Payne. (1990). Evanescent Field Amplification in a Tapered Single-Mode Optical Fibre. *Electronics Letters*, Vol. 26, 2, pp. 130-132

Malins, C., M. Landl, et al. (1998). Fibre Optic Ammonia Sensor Employing Novel Near Infrared Dyes. *Sensors and Actuators B*, Vol. 51, pp. 359-367

Maragos, C. M. and V. S. Thompson. (1999). Fiber-Optic Immunosensor for Mycotoxins. *Natural Toxins*, Vol. 7, pp. 371-376

Marazuela, M. D. and M. C. Moreno-Bondi. (2002). Fiber-Optic Biosensors: An Overview. *Analytical and Bioanalytical Chemistry*, Vol. 372, pp. 664-682

Marcuse, D. (1988). Launching Light into Fiber Cores from Sources Located in the Cladding. *Journal of Lightwave Technology*, Vol. 6, 8, pp. 1273-1279

McBee, T. W., L.-Y. Wang, et al. (2006). Characterization of Proton Transport Across a Waveguide-Supported Lipid Bilayer. *Journal of the American Chemical Society*, Vol. 128, 7, pp. 2184-2185

McCormack, T., G. O'Keeffe, et al. (1997). Optical Immunosensing of Lactate Dehydrogenase (LDH). *Sensors and Actuators B*, Vol. 41, pp. 89-96

McCreery, R. L., M. Fleischmann, et al. (1983). FIBER OPTIC PROBE FOR REMOTE RAMAN SPECTROMETRY. *Analytical Chemistry*, Vol. 55, 1, pp. 146-148

McDonagh, C., C. S. Burke, et al. (2008). Optical Chemical Sensors. *Chemical Reviews*, Vol. 108, pp. 400-422

McElvain, J., H. Antoniadis, et al. (1996). Formation and Growth of Black Spots in Organic Light-Emitting Diodes. *Journal of Applied Physics*, Vol. 80, pp. 6002-6007

Mignani, A. G., R. Falciai, et al. (1998). Evanescent Wave Absorption Spectroscopy by Means of Bi-Tapered Multimode Optical Fibers. *Applied Spectroscopy*, Vol. 52, 4, pp. 546-551

Mo, J., W. Zheng, et al. (2009). High Wavenumber Raman Spectroscopy for in Vivo Detection of Cervical Dysplasia. *Analytical Chemistry*, Vol. 81, 21, pp. 8908-8915

Monk, D. J., T. H. Ridgway, et al. (2002). Spectroelectrochemical Sensing Based on Multimode Selectivity Simultaneously Achievable in a Single Device. 15. Development of Portable Spectroelectrochemical Instrumentation. *Electroanalysis*, Vol. 15, 14, pp. 1198-1203

Monk, D. J. and D. R. Walt. (2004). Optical Fiber-Based Biosensors. *Analytical and Bioanalytical Chemistry*, Vol. 379, pp. 931-945

O'Keeffe, G., B. D. MacCraith, et al. (1995). Development of a LED-Based Phase Fluorimetric Oxygen Sensor Using Evanescent Wave Excitation of a Sol-Gel Immobilized Dye. *Sensors and Actuators B*, Vol. 29, pp. 226-230

Oroszlan, P., G. L. Duveneck, et al. (1993). Fiber-Optic Atrazine Immunosensor. *Sensors and Actuators B*, Vol. 11, pp. 301-305

Pandey, P. C. and H. H. Weetall. (1995). Detection of Aromatic Compounds Based on DNA Intercalation Using a Evanescent Wave Biosensor. *Analytical Chemistry*, Vol. 67, pp. 787-792

Plowman, T. E., S. S. Saavedra, et al. (1998). Planar Integrated Optical Methods for Examining Thin-Films and Their Surface Adlayers. *Biomaterials*, Vol. 19, pp. 341-355

Poscio, P., C. Depeursinge, et al. (1990). Realization of a Miniaturized Optical Sensor for Biomedical Applications. *Sensors and Actuators A*, Vol. 23, 1-3, pp. 1092-1096

Potyrailo, R. A. and G. M. Hieftje. (1998). Distributed Fiber-Optic Chemical Sensor with Chemically Modified Plastic Cladding. *Applied Spectroscopy*, Vol. 52, 8, pp. 1092-1095

Potyrailo, R. A. and G. M. Hieftje. (1998). Oxygen Detection by Fluorescence Quenching of Tetraphenylporphyrin Immobilized in the Original Cladding of an Optical Fiber. *Analytica Chimica Acta*, Vol. 370, pp. 1-8

Potyrailo, R. A. and G. M. Hieftje. (1999). Use of the Original Silicone Cladding of an Optical Fiber as a Reagent-Immobilization Medium for Intrinsic Chemical Sensors. *Fresenius Journal of Analytical Chemistry*, Vol. 364, pp. 32-40

Potyrailo, R. A., S. E. Hobbs, et al. (1998). Optcal Waveguide Sensors in Analytical Chemistry: Today's Instrumentation, Applications and Trends for Future Development. *Fresenius Journal of Analytical Chemistry*, Vol. 362, pp. 349-373

Potyrailo, R. A., S. E. Hobbs, et al. (1998). Optical waveguide sensors in analytical chemistry: today's instrumentation, applications and trends for future development. *Fresenius Journal of Analytical Chemistry*, Vol. 362, 4, pp. 349-373

Preejith, P. V., C. S. LIm, et al. (2003). Total Protein Measurement Using a Fiber-Optic Evanescnet Wave-Based Biosensor. *Biotechnology Letters*, Vol. 25, pp. 105-110

Reichert, W. M. (1989). Evanescent Detection of Adsorbed Films: Assessment of Optical Considerations for Absorbance and Fluorescence Spectroscopy at the Crystal/Solution and Polymer Solution Interfaces. *Critical Reviews in Biocompatibility*, Vol. 5, 2, pp. 173-205

Rogers, K. R., M. E. Eldefrawi, et al. (1991). Pharmacological Specificity of a Nicotinic Acetylcholine Receptor Optical Sensor. *Biosensors and Bioelectronics*, Vol. 6, pp. 507-516

Rogers, K. R., J. J. Valdes, et al. (1989). Acetylcholine Receptor Fiber-Optic Evanescent Fluorosensor. *Analytical Biochemistry*, Vol. 182, pp. 353-359

Ruddy, V., B. D. MacCraith, et al. (1990). Evanescent Wave Absorption Spectroscopy Using Multimode Fibers. *Journal of Applied Physics*, Vol. 67, 10, pp. 6070-6074

Samuel, I. D. W. and G. A. Turnbull. (2007). Organic Semiconductor Lasers. *Chemical Reviews*, Vol. 107, 4, pp. 1272-1295

Shaw, M. J. and W. E. Geiger. (1996). A New Approach to Infrared Spectroelectrochemistry Using a Fiber-Optic Probe: Application to Organometallic Redox Chemistry. *Organometallics*, Vol. 15, pp. 13-15

Shriver-Lake, L. C., J. P. Golden, et al. (1995). Use of Three Longer-Wavelength Fluorophores with the Fiber-Optic Biosensor. *Sensors and Actuators B*, Vol. 29, pp. 25-30

Smith, E. and G. Dent, Eds. (2005). *Modern Raman Spectroscopy: a practical approach*, John Wiley and Sons Ltd, Chichester

Stegemiller, M. L., W. R. Heineman, et al. (2003). Spectroelectrochemical Sensing Based on Multimode Selectivity Simultaneously Achievable in a Single Device. 11. Design and Evaluation of a Small Portable Sensor for the Determination of Ferrocyanide in Hanford Waste Samples. *Environmental Science and Technology*, Vol. 37, pp. 123-130

Stokes, D. L. and T. Vo-Dinh. (2000). Development of an integrated single-fiber SERS sensor. *Sensors and Actuators B-Chemical*, Vol. 69, 1-2, pp. 28-36

Stokes, D. L., Z. H. Chi, et al. (2004). Surface-enhanced-Raman-scattering-inducing nanoprobe for spectrochemical analysis." *Applied Spectroscopy*, 58(3): 292-298

Sutherland, R. M., C. Dahne, et al. (1984). Optical Detection of Antibody-Antigen Reactions at a Glass-Liquid Interface. *Clinical Chemistry*, Vol. 30, 9, pp. 1533-1538

Tai, H., H. Tanaka, et al. (1987). Fiber-Optic Evanescent-Wave Methane-Gas Sensor Using Optical Absorption for the 3.392-micron Line of a He-Ne Laser. *Optics Letters*, Vol. 12, 6, pp. 437-439

Taitt, C. R., G. P. Anderson, et al. (2005). Evanescent Wave Fluorescence Biosensors. *Biosensors and Bioelectronics*, Vol. 20, pp. 2470-2487

Thompson, R. B. (2006). *Fluorescence Sensors and Biosensors* Taylor and Francis, Boca Raton

Thompson, V. S. and C. M. Maragos. (1996). Fiber-Optic Immunosensor for the Detection of Fumonisin B_1. *Journal of Agricultural and Food Chemistry*, Vol. 44, pp. 1041-1046

Tien, P. K. (1971). Light Waves in Thin Films and Integrated Optics. *Applied Optics*, Vol. 10, 11, pp. 2395-2413

Tiwari, V. S., R. R. Kalluru, et al. (2007). Fiber optic Raman sensor to monitor the concentration ratio of nitrogen and oxygen in a cryogenic mixture. *Applied Optics*, Vol. 46, 16, pp. 3345-3351

Toppozada, A. R., J. Wright, et al. (1997). Evaluation of a Fiber Optic Immunosensor for Quantitating Cocaine in Coca Leaf Extracts. *Biosensors and Bioelectronics*, Vol. 12, 2, pp. 113-124

VanDyke, D. A. and H.-Y. Cheng. (1988). Fabrication and Characterization of a Fiber-Optic Based Spectroelectrochemical Probe. *Analytical Chemistry*, Vol. 60, pp. 1256-1260

Villatoro, J., D. Luna-Moreno, et al. (2005). Optical Fiber Hydrogen Sensor for Concentrations Below the Lower Explosive Limit. *Sensors and Actuators B*, Vol. 110, pp. 23-27

Vo-Dinh, T., D. L. Stokes, et al. (1999). Surface-enhanced Raman scattering (SERS) method and instrumentation for genomics and biomedical analysis. *Journal of Raman Spectroscopy*, Vol. 30, 9, pp. 785-793

Walczak, I. M., W. F. Love, et al. (1992). The Application of Evanescent Wave Sensing to a High-Sensitivity Fluoroimmunoassay. *Biosensors and Bioelectronics*, Vol. 7, pp. 39-48

Wang, Y., S. Guo, et al. (2008). Facile fabrication of large area of aggregated gold nanorods film for efficient surface-enhanced Raman scattering. *Journal of Colloid and Interface Science*, Vol. 318, 1, pp. 82-87

Wei, Z. Q., A. J. Mieszawska, et al. (2004). Synthesis and manipulation of high aspect ratio gold nanorods grown directly on surfaces. *Langmuir*, Vol. 20, 11, pp. 4322-4326

Wei, Z. Q. and F. P. Zamborini. (2004). Directly monitoring the growth of gold nanoparticle seeds into gold nanorods. *Langmuir*, Vol. 20, 26, pp. 11301-11304

Wiejata, P. J., P. M. Shankar, et al. (2003). Fluorescent Sensing Using Biconical Tapers. *Sensors and Actuators B*, Vol. 96, pp. 315-320

Willets, K. A. and R. P. Van Duyne. (2007). Localized surface plasmon resonance spectroscopy and sensing. *Annual Review of Physical Chemistry*, Vol. 58, pp. 267-297

Winograd, N. and T. Kuwana. (1969). Characteristics of the Electrode-Solution Interface Under Faradaic and Non-Faradaic Conditions as Observed by Internal Reflection Spectroscopy. *Journal of Electroanalytical Chemistry*, Vol. 23, 3, pp. 333-342

Wolfbeis, O. S. (2006). Fiber-Optic Chemical Sensors and Biosensors. *Analytical Chemistry*, Vol. 78, pp. 3859-3874

Xu, H. X., E. J. Bjerneld, et al. (1999). Spectroscopy of single hemoglobin molecules by surface enhanced Raman scattering. *Physical Review Letters*, Vol. 83, 21, pp. 4357-4360

Zhang, Y., C. Gu, et al. (2005). Surface-enhanced Raman scattering sensor based on D-shaped fiber. *Applied Physics Letters*, Vol. 87, 12,

Zhang, Z. Y., Q. Jiang, et al. (2009). A p-type-doped Quantum Dot Superluminescent LED with Broadband and Flat-Topped Emission Spectra Obtained by Post-Growth Intermixing Under a GaAs Proximity Cap. *Nanotechnology*, Vol. 4, pp. 055204-055208

Zhou, C., P. Pivarnik, et al. (1997). A Compact Fiber-Optic Immunosensor for *Salmonella* Based on Evanescent Wave Excitation. *Sensors and Actuators B*, Vol. 42, pp. 169-175

Recent Progress in Optical Fiber Research

Edited by Dr Moh. Yasin

ISBN 978-953-307-823-6

Hard cover, 450 pages

Publisher InTech

Published online 25, January, 2012

Published in print edition January, 2012

This book presents a comprehensive account of the recent progress in optical fiber research. It consists of four sections with 20 chapters covering the topics of nonlinear and polarisation effects in optical fibers, photonic crystal fibers and new applications for optical fibers. Section 1 reviews nonlinear effects in optical fibers in terms of theoretical analysis, experiments and applications. Section 2 presents polarization mode dispersion, chromatic dispersion and polarization dependent losses in optical fibers, fiber birefringence effects and spun fibers. Section 3 and 4 cover the topics of photonic crystal fibers and a new trend of optical fiber applications. Edited by three scientists with wide knowledge and experience in the field of fiber optics and photonics, the book brings together leading academics and practitioners in a comprehensive and incisive treatment of the subject. This is an essential point of reference for researchers working and teaching in optical fiber technologies, and for industrial users who need to be aware of current developments in optical fiber research areas.

InTech Europe
University Campus STeP Ri
Slavka Krautzeka 83/A
51000 Rijeka, Croatia
Phone: +385 (51) 770 447
Fax: +385 (51) 686 166
www.intechopen.com

InTech China
Unit 405, Office Block, Hotel Equatorial Shanghai
No.65, Yan An Road (West), Shanghai, 200040, China
中国上海市延安西路65号上海国际贵都大饭店办公楼405单元
Phone: +86-21-62489820
Fax: +86-21-62489821

IntechOpen